Adaptive control of an active seat for occupant vibration reduction

Zengkang Gan[a]*, Andrew J. Hillis[a], Jocelyn Darling[a]

[a] *Centre for Power Transmission and Motion Control, Department of Mechanical Engineering, University of Bath, Claverton Down, Bath, BA2 7AY, United Kingdom*

*** Corresponding author:** Z. Gan, Tel.: +44(0)1225 38 4019, E-mail: zengkang.gan@hotmail.com

Abstract

The harmful effects on human performance and health caused by unwanted vibration from vehicle seats are of increasing concern. This paper presents an active seat system to reduce the vibration level transmitted to the seat pan and the occupants' body under low frequency periodic excitation. Firstly, the detail of the mechanical structure is given and the active seat dynamics without external load are characterized by vibration transmissibility and frequency responses under different excitation forces. Owing the non-linear and time-varying behaviour of the proposed system, a Filtered-x least-mean-square (FXLMS) adaptive control algorithm with on-line Fast-block LMS (FBLMS) identification process is employed to manage the system operation for high vibration cancellation performance. The effectiveness of the active seat system is assessed through real-time experimental tests using different excitation profiles. The system identification results show that an accurate estimation of the secondary path is achieved by using the FBLMS on-line technique. Substantial reduction is found for cancelling periodic vibration containing single and multiple frequencies. Additionally, the robustness and stability of the control system are validated through transient switching frequency tests.

Keywords: active vibration control; active seat; adaptive algorithms; on-line system identification; electromagnetic actuator.

1. Introduction

Vehicle occupants are typically exposed to unpleasant whole body vibration for extended period of time. It is well known that the transmission of unwanted vibration to the human body can lead to fatigue and discomfort. Moreover, the unwanted vibration normally distributed in the low-frequency range (0.5-25 Hz), has been found as the main risk factor for lower back pain and lumbago [1-3], which seriously affect the mental and physical health of occupants and influence their working performance. Since it is much more difficult and more energy-consuming to successfully reduce the vibration level globally than locally on vehicles, vibration cancelation on seats – the part which directly contacts with the human, has attracted considerable interest in recent years. So far, for most vehicle seats, vibration isolation is achieved passively by using seat cushions and fixed load energy absorbers, which have limited performance in the low frequency range. In addition, the impedance properties of the conventional passive seat cushions and energy absorbers are difficult to optimize due to the varying conditions. In contrast, semi-active or fully active seat suspensions are able to provide sufficient vibration isolation in low frequency range and address the variation in disturbance.

In recent years, many researchers have been working on the vibration isolation problem for vehicle seats and various approaches have been proposed. Wu and Griffin [4] developed a semi-active seat suspension using an electro-rheological (ER) fluid damper to reduce the seat impacts caused by shocks or high magnitude vibration. Choi et al. [5] proposed a semi-active seat suspension using a magneto-rheological (MR) fluid damper for commercial vehicles. McManus et al. [6] evaluated the vibration and shock attenuation performance of a semi-active MR fluid damper in reducing the incidence and severity of end-stop impacts of a low natural frequency suspension seat. Hiemenz et al. [7] explored the use of a MR damper in a semi-active seat suspension system for helicopter crew seats to enhance occupant comfort. It has been found that semi-active systems provide some desirable benefits, such as being easy to implement and control. However, the force range of semi-active system is limited, and they are known to be 'soft' to high frequency excitations while being 'stiff' to low frequency excitations [11]. Therefore, the vibration isolation performance in the low frequency range can be compromised.

Active seat suspensions which can provide much wider force range and achieve better isolation performance in low frequency region have attracted more and more attention in recent years. For instance, Kawana and Shimogo [8] proposed an active seat suspension for a heavy duty truck using an electric servo-motor and ball-screw mechanism which showed that some resistance will remain even if the control is off. Stein [9] developed an electro-pneumatic active seat suspension for a driver's seat for heavy earth moving equipment or off-road vehicles. Maciejewski et al. [10] presented an active seat suspension system containing a controlled pneumatic spring and a hydraulic shock-absorber. The active control of air-flow to the pneumatic spring was applied by means of a directional servo-valve. There are some drawbacks in pneumatic systems: They require large amount of energy to maintain the necessary air pressure in the source, and the complexity of the systems make them less reliable and difficult to control. In a recent study by Chen et al. [11], an adaptive helicopter seat mount using stacked piezoelectric actuators was developed. The seat mount has been retrofitted on a full-scale Bell-412 helicopter co-pilot seat and the performance was evaluated through closed-loop tests. The results showed that significant vibration suppression was achieved. However, the study also found that the stacked piezoelectric actuators can't provide enough stroke to effectively suppress the low frequency vibration.

Besides the numerous proposed active seat suspensions, a number of control approaches have been developed. Li et al. [12] designed a fuzzy H-infinity controller based on the Takafi-Sugeno (T-S) fuzzy model for active suspension systems with the consideration of actuator delays and faults. A nonlinear sliding control law has been applied to an active electro-hydraulic suspension system to improve the ride quality of the vehicle by Alleyne and Hedrick [13]. Since the controller relied on an accurate model of the suspension system, an adaptation scheme based on Lyapunov analysis was introduced. Aldair and Wang [14] designed a neurofuzzy (NF) controller for active vehicle suspension systems to minimize vibration when travelling on a rough road. A control algorithm, based on a combination of robust and adaptive approaches has been investigated for an active driver's seat by Wu and Chen [15]. Maciejewski [16] used an active vibration control strategy for a pneumatic seat suspension based on the inverse dynamics of a force actuator and the primary controller. Fialho and Balas [17] presented an approach to the design of road adapting active suspensions via a combination of linear parameter-varying gain-scheduling and nonlinear backstepping techniques. Le and Ahn [18] proposed an adaptive intelligent backstepping controller (AIBC) for an active seat suspension for high vibration isolation effectiveness. In this controller, large uncertain parameters resulted in chattering in the control signal

and lead the system to instability. In addition, some other controllers also have been presented in [19-23].

As is known, active seat systems are usually subject to non-linear and time-varying behaviour. The use of a fully adaptive control strategy is required to maintain optimum isolation performance. Due largely to its simplicity and robustness, the LMS adaptive algorithm is the most popular control strategy for this type of application [19]. In this work, the FXLMS version of the algorithm has been applied to the proposed active seat to manage the system operation for high vibration cancellation performance. The remainder of the paper is organized as follows: the active seat mechanical structure and dynamic characteristics are given in Section 2. The FXLMS adaptive control algorithm and the FBLMS on-line system identification technique are described in Section 3. The experimental apparatus is illustrated in Section 4, while the experimental results are shown in Section 5. Finally the conclusions are drawn in Section 6.

2. Active seat structure and dynamics

2.1 Active seat structure

A proof-of-concept active seat was designed and built on the basis of the required high vibration isolation performance in low frequency excitation ranges. The mechanical model of the active seat is shown in Fig. 1. The seat includes a passive suspension and an active actuation system. The passive suspension which is composed of a spring and damper can take off the main static load of the seat pan and occupant. The active actuation system is composed of two electromagnetic linear actuators which are installed in parallel at the front and the rear of the seat pan to provide active control authority. The moveable seat pan is supported at the middle of both sides by a two-bar lever mechanism. At the rear of the seat pan, two linear sliders are used to allow the seat pan to move along the seat base vertically (±3 cm approximately). The linear rails are rigidly mounted on each side of the seat base and the linear carriages are connected to the seat pan via ball bearings. The vertical motion of the seat pan is illustrated using dashed lines in Fig. 1.

The detail of the active seat structure is given by the three-dimension line drawings shown in Fig. 2. An Elka-stage-5 shock absorber which consists of a steel coil spring and an adjustable damper was selected as the passive suspension element. Two XTA-3806 electromagnetic linear actuators manufactured by the Dunkermotoren GmbH were chosen as the active struts.

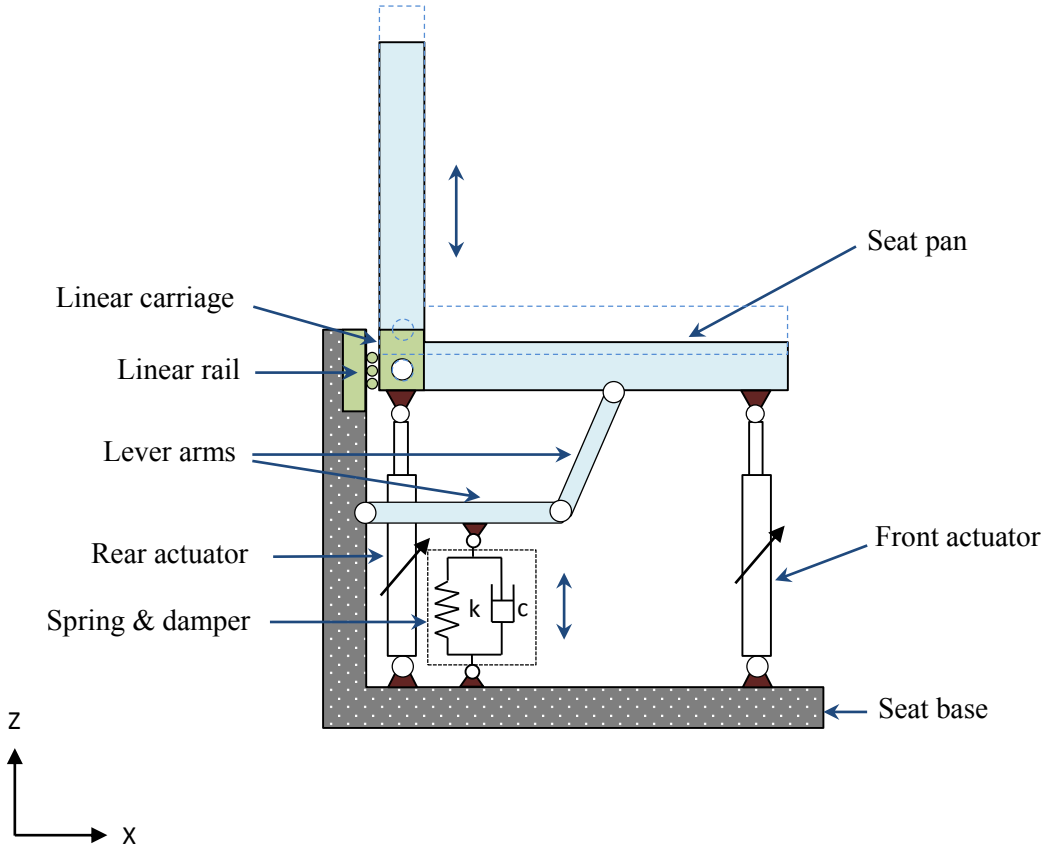

Fig. 1. Mechanical model of the active seat.

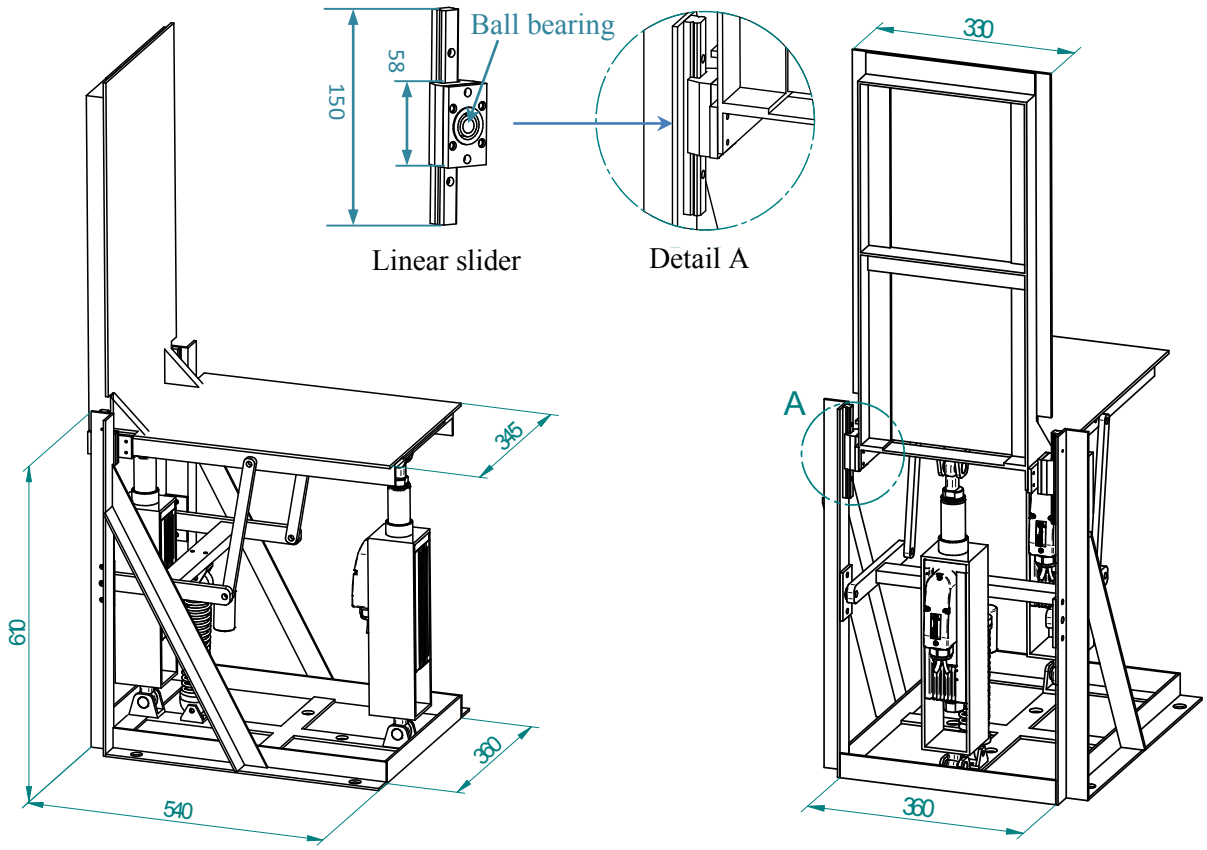

Fig. 2. Line drawings of the active seat.

2.2 Active seat dynamics

Experimental tests were carried out to identify the dynamic characteristics of the active seat. As shown in Fig. 3, the vibration transmissibility from the seat base to the seat pan without external load and with actuators powered off was calculated. This was obtained by measuring the acceleration level at the seat base and the seat pan simultaneously under sinusoidal excitation in the frequency range of 1-25 Hz with a frequency interval of 0.5 Hz. The transmissibility curve reveals a dominant resonant frequency between 10 and 14 Hz, and the associated peak magnitude is over 2.

Fig. 4 shows the magnitude and phase responses of the active seat under the excitation force generated by the two actuators. Sinusoidal signals starting from 0.5 Hz to 25 Hz with a frequency interval of 0.5 Hz are used to drive the actuators. Three different force levels: peak values at 55.8 N, 83.7 N and 111.6 N for each actuator, were chose for the response test. It can be observed that there are distinctive peaks in the magnitude response curves between the 10-20 Hz frequency range, and these are due to the resonance near the fundamental frequency of the active seat. It is also found that the frequency range of the resonance tends to broaden as the excitation force increases. The phase responses show a general good consistency below 10 Hz and a bigger difference between 10 Hz and 25 Hz. This is caused by the non-linearity of the seat system. Moreover, the fundamental frequency of the active seat increases compared with those revealed by the transmissibility curve, shown in Fig. 3, when the actuators are powered off. This is because that the overall dynamic stiffness of the system is increased by the added force when the actuators are powered on.

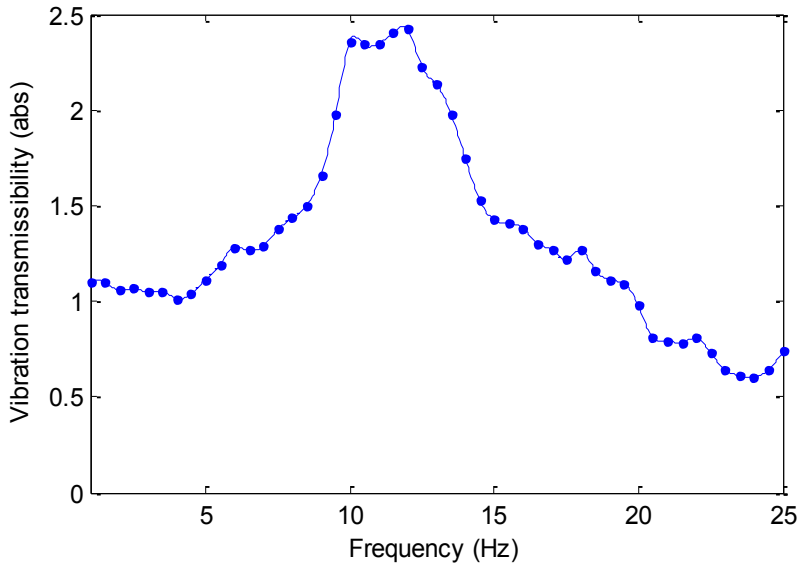

Fig. 3. Vibration transmissibility from the seat base to the seat pan without external load.

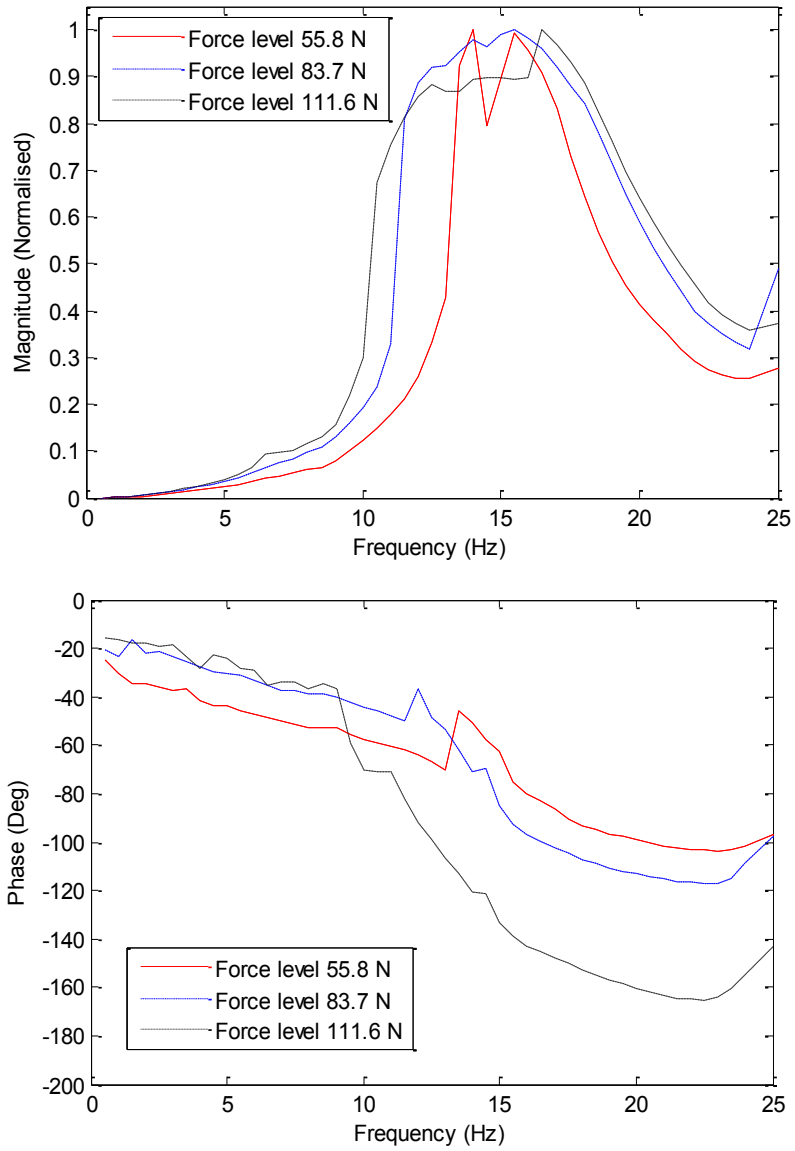

Fig. 4. Magnitude and phase responses of the active seat under the actuator excitation force.

From the above dynamic analysis, it can be seen that the active seat system is subject to non-linear behaviour. Furthermore, the system is also influenced by the time-varying effects which would result from the external load disturbance (i.e. occupant's weight variations), temperature changes and ageing of the system. Therefore, in order to achieve effective vibration suppression on the active seat an adaptive control method which can perform on-line system identification is required. In the next section, a LMS based adaptive algorithm will be introduced for the control of the active seat.

3. Adaptive control law

3.1 The FXLMS algorithm

The FXLMS algorithm is developed from the conventional LMS adaptive filter which was originally developed by Widrow and Hoff [24]. The detailed derivation and analysis of the LMS algorithm can be found in [24-26]. It has been widely applied in the field of active noise and vibration control and it has been found to offer robust and effective performance for periodic vibration attenuation. The block diagram of the FXLMS algorithm in an active vibration control (AVC) system is depicted in Fig. 5.

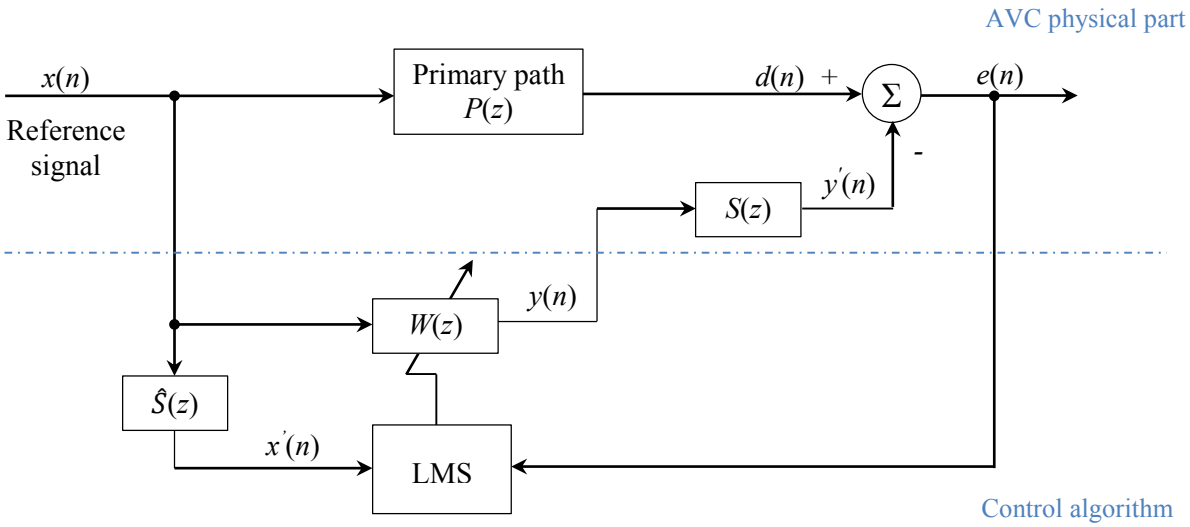

Fig. 5. Block diagram of the FXLMS algorithm in AVC system.

The primary path $P(z)$ is the plant between the vibration source and the error sensor, the adaptive filter $W(z)$ uses the LMS algorithm and the reference signal $x(n)$ to update its coefficients in order to estimate and track the changes of the primary path. The filter coefficients are updated to minimise a cost function based on the measured error signal $e(n)$ between the desired response and the filter output. The algorithm can reach a unique minimum (optimal performance) at the point of zero gradient. The filter output $y(n)$ drives the actuators to produce the cancellation force. The actuators, however, will introduce a secondary path dynamic $S(z)$ to the system. The added dynamics will result in a phase shift in the error signal $e(n)$, which will eventually cause instability. The FXLMS algorithm solves the problem by placing a plant $\hat{S}(z)$, the estimate of $S(z)$, in the reference signal path before the weight update of the LMS algorithm to compensate the secondary path effect.

3.2 Narrowband feed-forward FXLMS algorithm

Vibration for vehicle seats can be generally divided into broadband and narrowband according to the energy distribution across the frequency band. Broadband vibration on vehicle seats can be introduced by rough road profiles, while narrowband vibration can result from periodic engine vibration and aerodynamics. For instance, helicopter seat vibration is dominated by the N/rev harmonics which are introduced by the rotor aerodynamic load [11]. In experimental studies, active narrowband periodic vibration cancellation was evaluated on the active seat. Fig. 6 shows the implementation of the narrowband feed-forward FXLMS algorithm with the active seat.

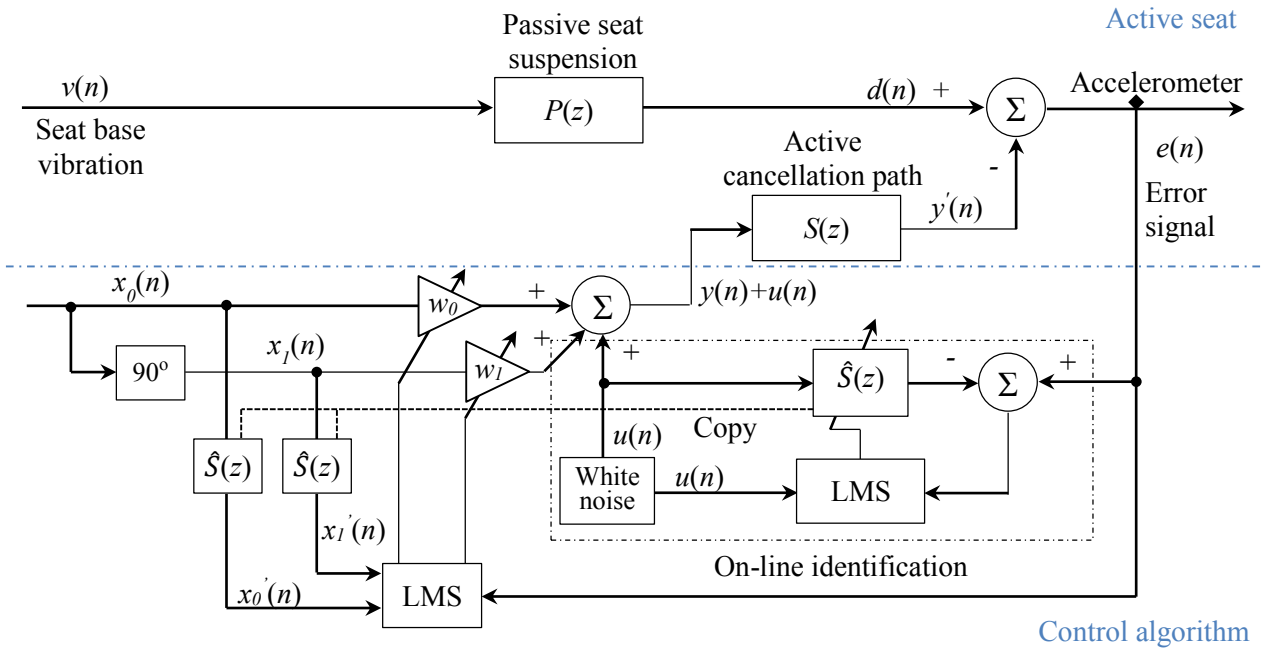

Fig. 6. Implementation of the narrowband feed-forward FXLMS algorithm on the active seat.

As shown in Fig. 6, the seat base vibration $v(n)$ is transmitted through the primary path dynamic $P(z)$, representing the passive seat suspension. The output of the primary plant $d(n)$ is the primary vibration on the active seat, which is to be cancelled. The secondary path $S(z)$ represents the dynamics of the active cancellation section which include the actuators, the vibration path to the feedback sensor and a band-pass filter. The error signal $e(n)$ is the resultant acceleration measured by an accelerometer.

Below the dashed line is the control algorithm. Two synthesised orthogonal components $x_0(n)$ and $x_1(n)$ are used for the reference signals, which contain only the frequencies that require cancellation. The reference signals are defined by the equations:

$$\begin{aligned} x_0(n) &= A_0 \sin(\omega_e n\Delta t), \\ x_1(n) &= A_1 \cos(\omega_e n\Delta t), \end{aligned} \tag{1}$$

where A_0 and A_1 are the amplitudes, ω_e is the estimated vibration frequency which require cancellation, and Δt is the fixed sampling interval.

Two adaptive weights are required for every frequency present in the reference signals for cancellation. The weights are iterated by the equations:

$$\begin{aligned} w_0(n+1) &= \varepsilon w_0(n) - \mu x_0'(n) e(n), \\ w_1(n+1) &= \varepsilon w_1(n) - \mu x_1'(n) e(n), \end{aligned} \tag{2}$$

where x_0' and x_1' are the reference signals filtered by the secondary path estimate $\hat{S}(z)$, μ is the convergence rate (a positive real constant) of the algorithm, ε is a leakage factor chosen in the range $0< \varepsilon <1$, which is applied to avoid the accumulation of numerical rounding errors in the filter weights, and $e(n)$ is the error signal given by the equation:

$$e(n) = d(n) - y'(n) = v(n)p(n) - y(n)s(n) - u(n)s(n) \tag{3}$$

where $p(n)$ and $s(n)$ are the impulse response of $P(z)$ and $S(z)$ at time n, $y(n)$ is the filter output, $u(n)$ is a low-level white noise. The control signal for the actuators is the filter output $y(n)$ plus the noise $u(n)$ and it is expressed as follow:

$$y(n) + u(n) = w_0(n)x_0(n) + w_1(n)x_1(n) + u(n) \tag{4}$$

The low-level white noise $u(n)$ is introduced by the on-line system identification process. As mentioned in section 2, the active seat system is subject to non-linearity and time-varying effects, so it is necessary to perform on-line system identification in parallel with the cancellation algorithm.

3.3 On-line secondary path identification using FBLMS

The on-line secondary path $S(z)$ identification is achieved using an additional LMS filter, as shown in Fig. 6. A low-level white noise $u(n)$ is generated and added to the control signal to drive the actuators. The noise component is passed to the error signal $e(n)$ and fed back to the LMS filter to model $S(z)$. In practice, the measured residual error signal usually contains some components uncorrelated with the reference noise $u(n)$, which can cause problems with the on-line identification when using a time-domain filter [25]. The corrupted estimation of $S(z)$ can increase the convergence time of the cancellation filter and result in system instability. The FBLMS algorithm which operates in the frequency domain can solve this problem and substantially improve the robustness of the system identification. The block diagram of the FBLMS algorithm is shown in Fig. 7.

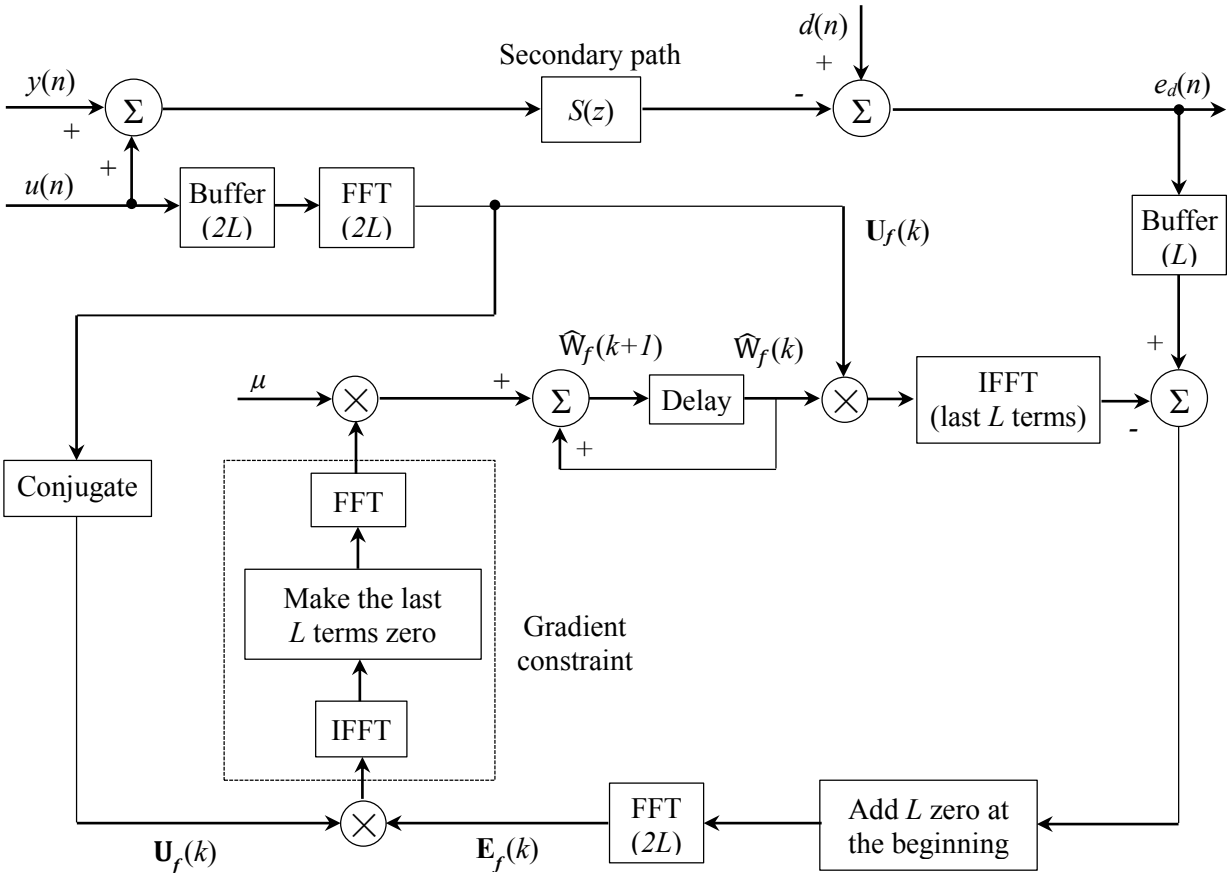

Fig. 7. Block diagram of the FBLMS algorithm for on-line secondary path identification [26].

In the FBLMS algorithm, the overlap-save method, which applies discrete Fourier transform (DFT), is used for efficient computation of linear convolution. It has been found that the use of 50 percent overlap (i.e. the block length equals to the filter weights length) is the most efficient.

The time-domain weight vector $\hat{\mathrm{w}}(k)$ with size of *L-by-1* is extended to *2L-by-1* vector $\hat{\mathrm{w}}_{\mathrm{e}}(\mathrm{k})$ by padding an equal size zero vector, and the frequency domain weight $\widehat{\mathrm{W}}_{\mathrm{f}}(\mathrm{k})$ is defined as:

$$\widehat{W}_f(k) = FFT[\hat{w}_e(k)\,] = FFT\begin{bmatrix}\hat{\mathrm{w}}(k)\\ \mathbf{0}\end{bmatrix} \tag{5}$$

where k denotes the block index. The weight $\widehat{\mathrm{W}}_f(k)$ recursion is obtained as:

$$\begin{aligned}\widehat{W}_f(k+1) &= \widehat{W}_f(k) + \mu FFT\begin{bmatrix}\rho(k)\\ \mathbf{0}\end{bmatrix}\\ \rho(k) &= P_{L,0}IFFT[\mathbf{U}_f(k)\mathbf{E}_f(k)]\end{aligned} \tag{6}$$

where $P_{L,0}$ is a *2L-by-2L* windowing matrix which ensures that the last L terms of the updated weight vector $\widehat{\mathrm{W}}_f(k+1)$ remain zero, $\mathbf{E}_f(k)$ is the frequency domain error signal, $\mathbf{U}_f(k)$ is obtained by taking FFT of the two successive blocks of noise signal *u(n)* and is expressed as:

$$\mathbf{U}_f(k) = diag\{FFT[u(kL-L),\dots,u(kL-1),u(k),\dots,u(kL+L-1)]\} \tag{7}$$

where $diag$ donates an L-by-L diagonal matrix.

The convergence rate of the FBLMS algorithm can be improved by using the step-normalization technique, which is achieved by assigning individually normalized step-size parameters to each element of the weight vector $\widehat{\mathrm{W}}_f(k)$. The step-size parameter μ becomes a function of the power spectral density (PSD) of the reference signal. However, it is a function of the PSD of the measured error signal for this application.

$$\mu_i(k) = \frac{\mu_0}{\boldsymbol{P}_i(k)},\ i = 0,1\dots,2L-1. \tag{8}$$

where μ_0 is a constant, k is the block number, $\boldsymbol{P}_i(k)$ are the power estimates of the samples of the filter input in the frequency domain and they can be obtained by using a first order low-pass filter as follows:

$$\boldsymbol{P}_i(k) = \beta\boldsymbol{P}_i(k-1) + (\mathbf{1}-\beta)|\,\mathrm{E}_{\boldsymbol{i}}\,(k)|^2,\ i = 0,1,\dots,2L-1. \tag{9}$$

where $E_{\boldsymbol{i}}\,(k)$ is the measured error applied to the i^{th} weight in the FBLMS algorithm, β is a forgetting factor chosen in the range $0 < \beta < 1$, and close to 1.

By using the step-normalization, a lower adaption rate is applied to the frequency bins containing signal power relating to the uncancelled seat vibration components and the corruption of the estimate $\hat{S}(z)$ is reduced.

3.4 Multiple harmonics cancellation using FXLMS

Multiple harmonic vibration cancellation has also been evaluated on the active seat, as the periodic vibration usually contains tones at the fundamental frequency plus several harmonics. The single frequency FXLMS algorithm can be extended to cancel multiple frequencies by adding additional controllers to each harmonic. For the case to cancel *M* harmonics in a periodic vibration, *M* two-weight adaptive filters can be applied in parallel. Fig. 8 shows the configuration of parallel narrowband AVC systems.

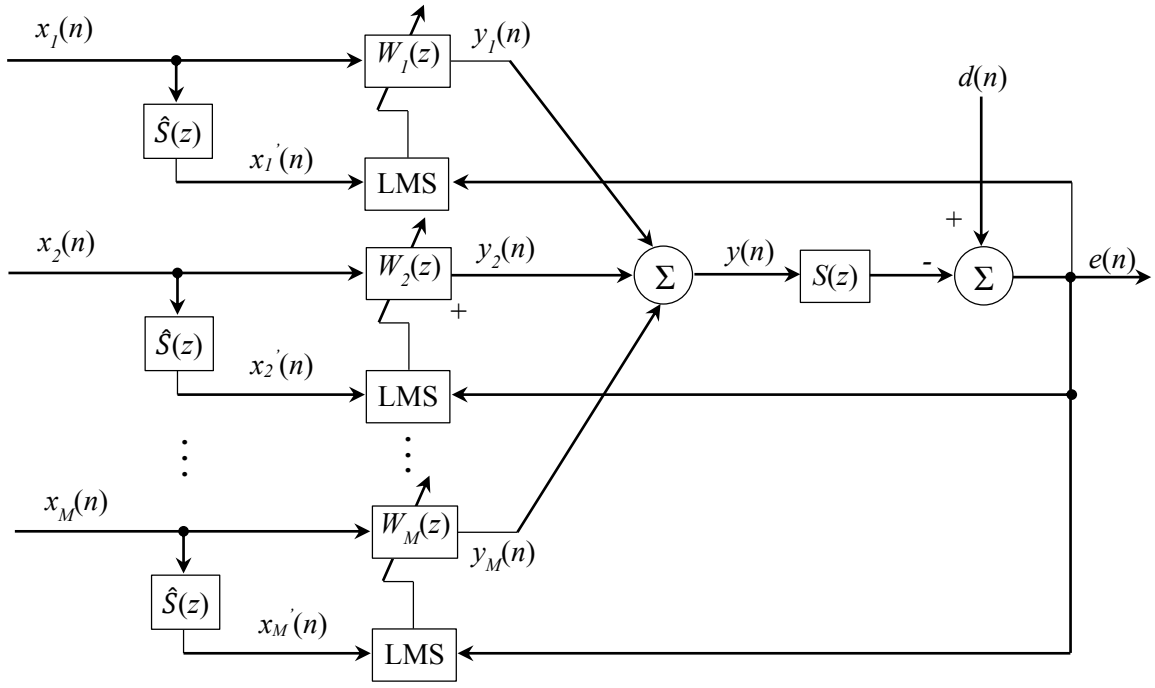

Fig. 8. Parallel narrowband AVC system for multiple frequencies cancellation.

The cancelling signal now is the sum of the *M* adaptive filter outputs as given by:

$$y(n) = \sum_{m=1}^{M} y_m\,(n),$$

$$y_m(n) = w_{m,0}(n)x_{m,0}'(n) + w_{m,1}(n)x_{m,1}'(n),\ m = 1,2,\dots,M. \tag{10}$$

where $x_{m,0}'(n)$ and $x_{m,1}'(n)$ are the filtered reference signals with 90 degrees phase shift.

In the experimental studies, the active seat has been tested by cancelling 4 harmonic frequencies in a periodic vibration signal. In addition, the transient performance of the system has been investigated using switching frequency signal containing 3 harmonics.

4. Experimental apparatus

In order to evaluate the control performance of the active seat, an experimental apparatus is established as shown in Fig. 9. The active seat is rigidly mounted on the platform of a multi-axis vibration simulation table (MAST). A vibration test dummy which has appropriate mass distribution and stiffness and damping coefficients is used as a seated human body substitute in the tests in order to ensure an improved consistency in behaviour and avoid safe and ethical issues. The dummy is secured on the seat using a standard seat belt and a chest strap. A total of four piezoresistive

accelerometers (Entran, EGCS-D1CM-25) are used to measure the acceleration and provide feedback signals. The mounting locations of the accelerometers are: the simulator platform (i.e. seat base), the middle of the seat pan, the dummy pelvis and the dummy shoulder. All the acceleration measurements are in the vertical direction. The I/O interface is a NI PCI-6229 board and the control algorithm is implemented on a xPC target system with a sampling rate of 1 kHz. The specification of the experimental apparatus is given in Table 1.

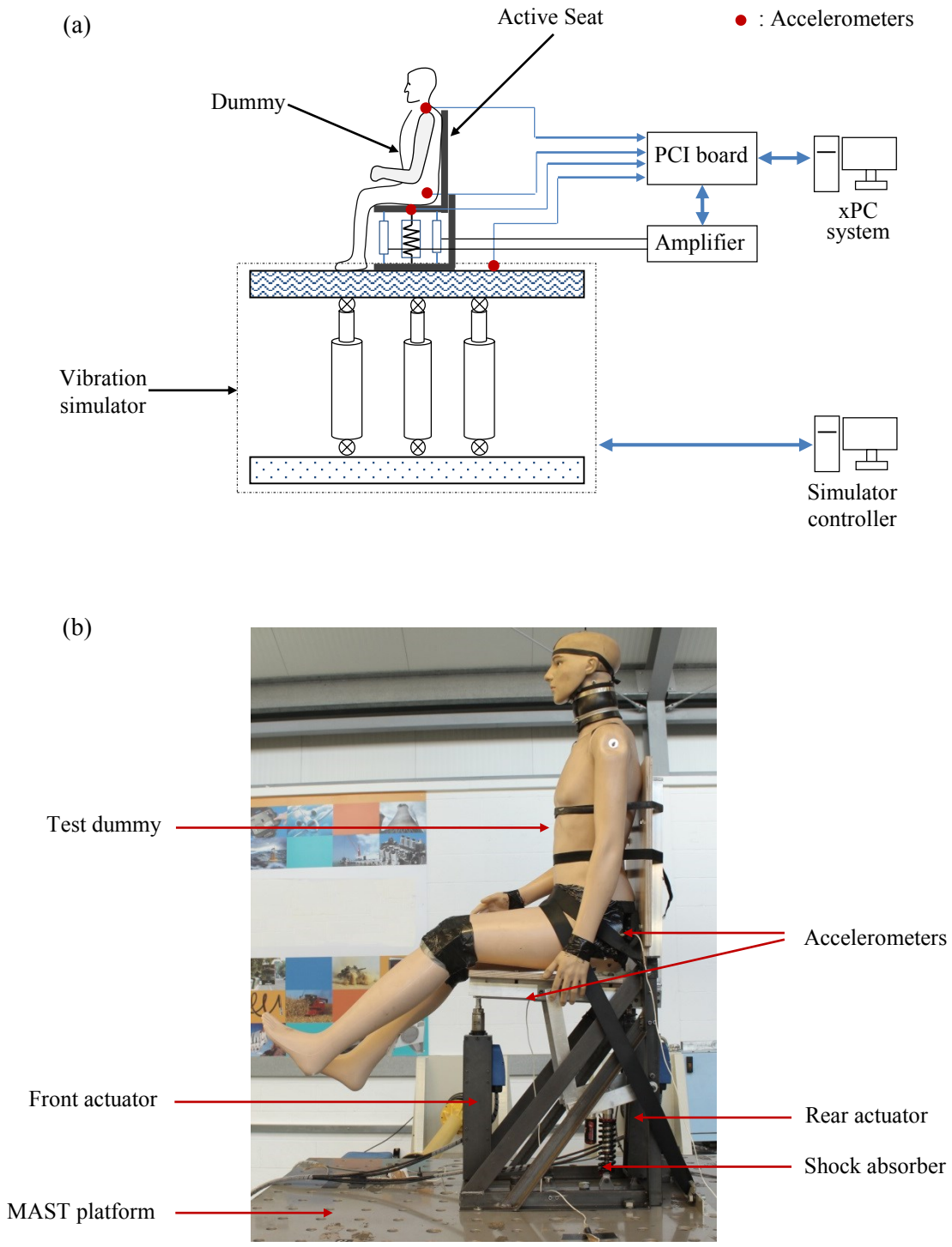

Fig. 9. The experimental apparatus.

Table 1

Experimental setup.

Number	Name	Specification
1	Actuator (XTA-3806)	Peak force: 1116 N Continuous stall force: 168.2 N Force constant: 78.9 N/Arms Peak acceleration: 313 ms^{-2} Maximum speed: 3.8 ms^{-1} Stroke: ±30 mm (Limited range)
2	MAST	Operational frequency range:0-50 Hz Stroke: ±75 mm Peak acceleration: 60 ms^{-2}
3	Test dummy	Mass: 55 kg (Seated human body mass supported by the seat)
4	Accelerometer (EGCS-D1CM-25)	Frequency response range: 0-240 Hz Sensitivity: 8 Mv/g Non-linearity: ±1% FSO
5	I/O board (NI PCI-6229)	16-Bit, 250 kS/s, 32 analog inputs and 4 analog ouputs

5. Experimental results

5.1 Secondary path identification

In the experimental studies, the residual vibration on the seat pan was selected as the error signal. The vibration on the dummy pelvis and shoulder has been measured and evaluated. In this case, the secondary path represents the dynamics from the control output to the residual acceleration, which is measured by the accelerometer located on the seat pan. The secondary path dynamics are estimated by using the FBLMS on-line identification method and the result is compared with that obtained by using standard system identification technique (Broad-band noise was employed to excite the system and the input and output were recorded and used to generate the frequency response), as shown in Fig. 10. The length of the adaptive filter is 128 and the sampling rate is 1 kHz. It is seen that good agreement is achieved between the magnitude response during the whole frequency range of interest, and the deviation in the phase response is insignificant apart from the very low frequency.

Fig.11 shows the comparison between the impulse test result and the offline and online identification results in the form of the filter impulse response. It can be seen that there is approximate 0.01 second (i.e. 10 samples) delay at the beginning of both the on-line and off-line FBLMS identification responses. The delay is eliminated around 0.01 second later and general good agreement is obtained. The comparison results show that the FBLMS on-line method is accurate and reliable for the secondary path identification.

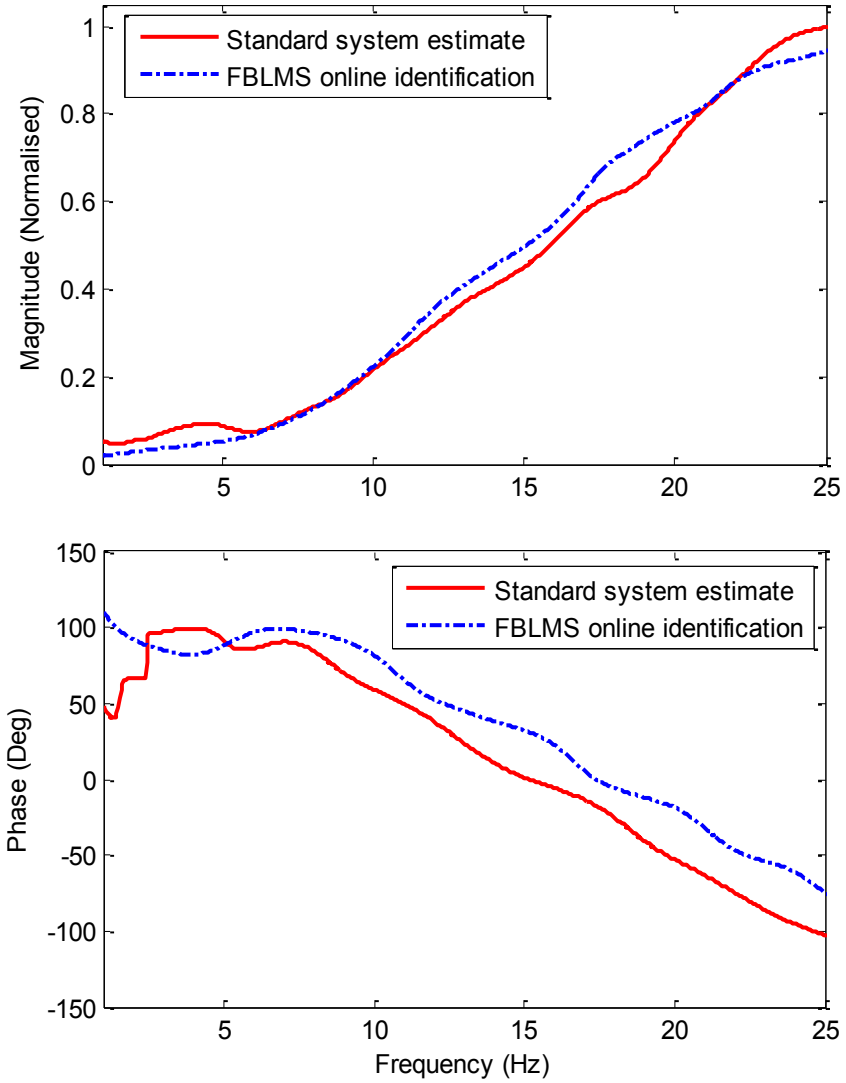

Fig. 10. Comparison between the estimated secondary path dynamics using FBLMS on-line identification technique and standard system identification method.

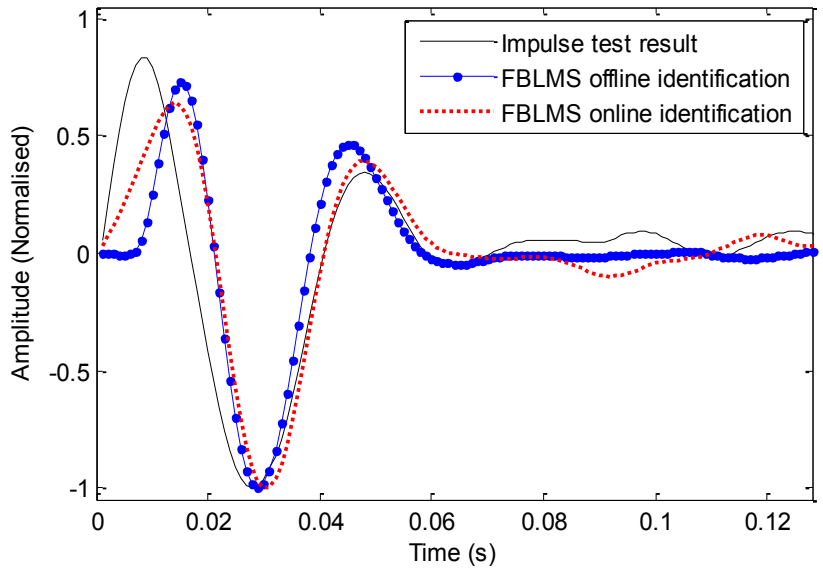

Fig. 11. Comparison between the impulse test result and the offline and online identification results in the form of the filter impulse response.

5.2 Single frequency cancellation

The performance of the active system was initially validated by cancelling a single frequency vibration. A 6 Hz disturbance with peak input acceleration approximately 0.1 g was applied to the system, and the vibration cancellation performance using FXLMS with on-line FBLMS identification is compared with the uncontrolled vibration on the three target locations: the seat pan (SP), the dummy pelvis (DP) and the dummy shoulder (DS). The cancellation results are the pseudo steady-state performance when the controller was fully adapted.

Fig. 12 shows the comparison results on the seat pan. It can be seen that around 26 dB cancellation is achieved at the frequency of 6 Hz. However, some low level random noise was introduced by the on-line identification process.

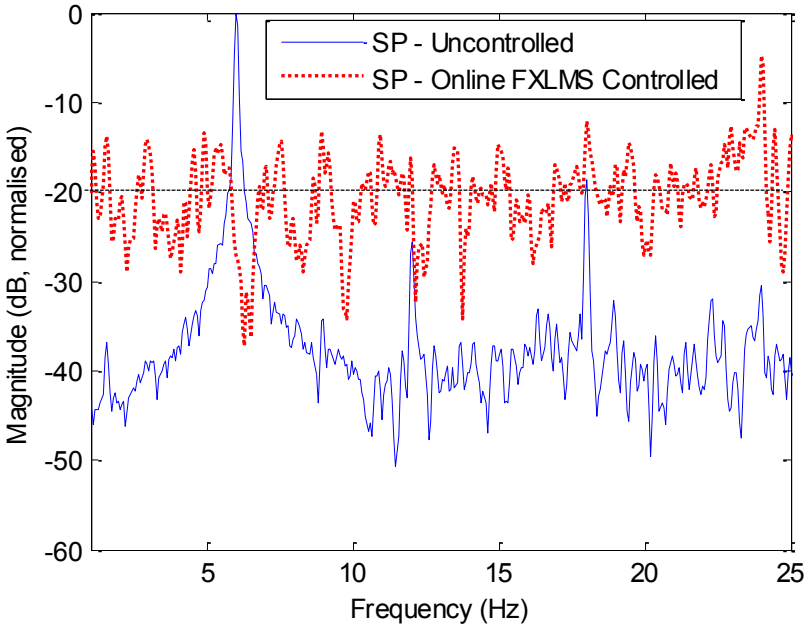

Fig. 12. Single frequency cancellation result on the seat pan.

Fig. 13 shows the comparison results on the dummy pelvis. It is seen that the vibration level is reduced more than 15 dB at the frequency of 6 Hz. Also, it can be observed that the introduced random noise is generally lower than that on the seat pan.

Fig. 14 shows the comparison results on the dummy shoulder. It can be seen that similar vibration reduction as on the dummy pelvis is achieved. However, some higher harmonics (the third harmonic 18 Hz and the forth harmonic 24 Hz) were observed. These are a result of the dummy dynamics being excited by the active cancellation force. In the experimental tests, a maximum active force limit was set to protect the system. The limit caused force saturation and thus excited some higher harmonics during the cancellation tests.

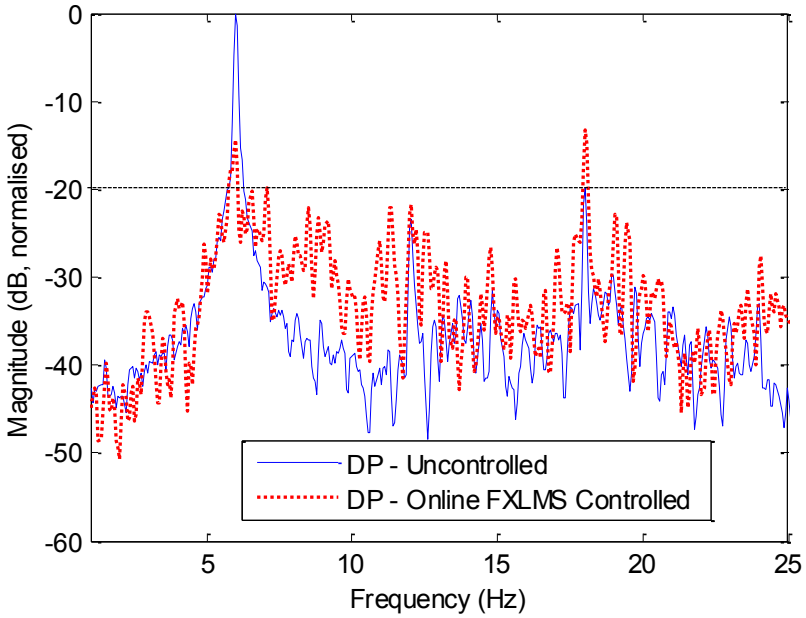

Fig. 13. Single frequency cancellation result on the dummy pelvis.

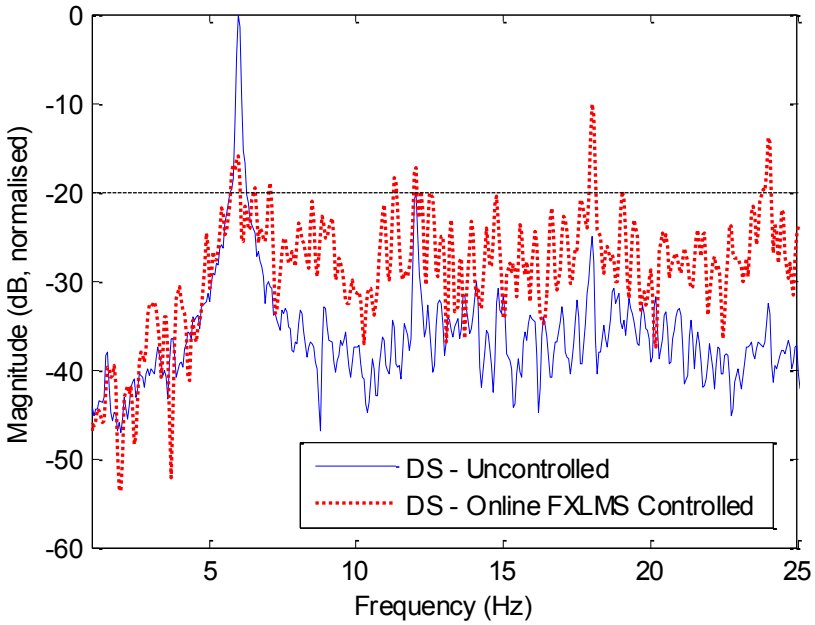

Fig. 14. Single frequency cancellation result on the dummy shoulder.

5.3 Multiple harmonics cancellation

A vibration signal containing four frequencies was used to excite the system, and the single frequency FXLMS algorithm was extended to cancel each frequency component by adding additional sub-controllers. The selected four frequencies are 4 Hz and 6 Hz and their second harmonics 8 Hz and 12 Hz. The overall peak input acceleration is 0.1 g approximately. The cancellation results are presented in the following figures. Again, they are the pseudo steady-state performances when the controllers were fully adapted.

Fig. 15 shows the harmonics cancellation results on the seat pan. It can be found that the average level of vibration cancellation achieved is around 20 dB at 4 Hz, 6 Hz and 8 Hz, and at 12 Hz is around 5 dB. This demonstrates the effectiveness of the active system for cancelling multiple harmonics vibration.

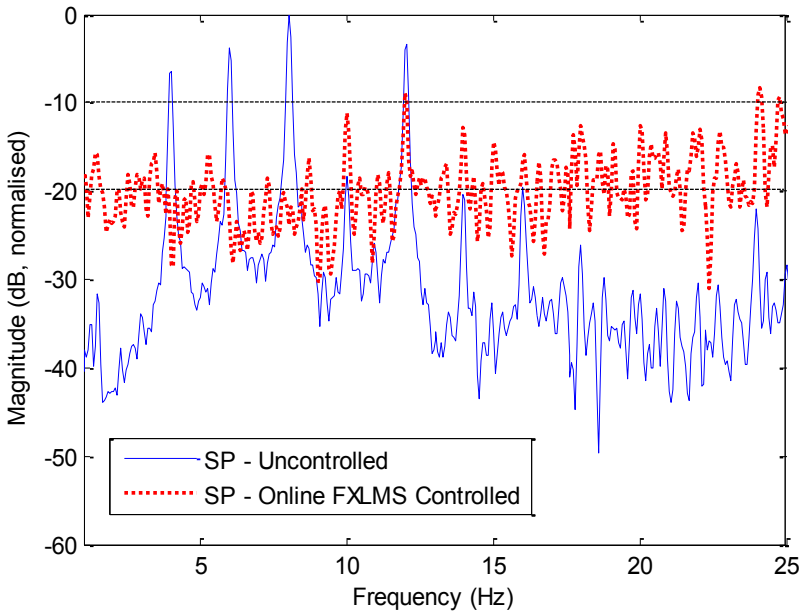

Fig. 15. Harmonics cancellation result on the seat pan.

Fig. 16 and 17 show the harmonics cancellation results on the dummy pelvis and shoulder, respectively. It can be seen that the vibration level on the dummy pelvis and shoulder is reduced to below -10 dB at all the harmonic frequencies and the maximum cancellation occurs at 6 Hz. Again, some additional harmonics at 10 Hz, 14 Hz, 18 Hz and 24 Hz can be observed on the dummy pelvis and shoulder cancellation plots. Again, these are a result of the dummy dynamics being excited by the active cancellation force.

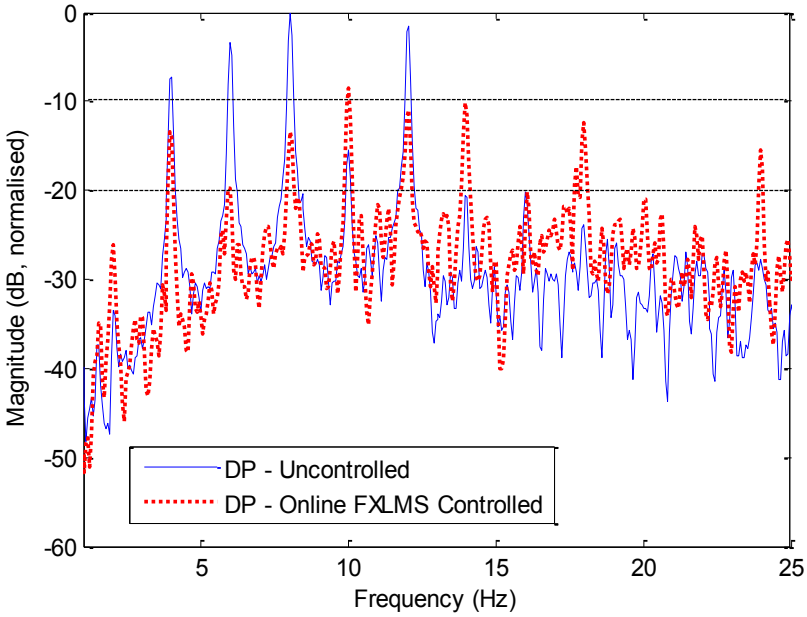

Fig. 16. Harmonics cancellation result on the dummy pelvis.

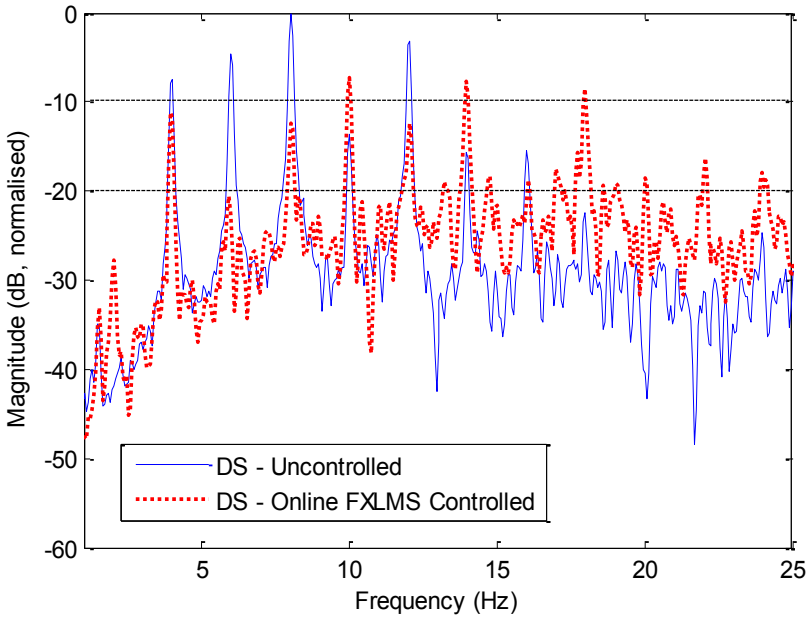

Fig. 17. Harmonics cancellation result on the dummy shoulder.

5.4 Transient switching frequency cancellation

Transient switching frequency cancellation tests were carried out to evaluate the speed of response and robustness of the active control system. The excitation vibration contains three frequencies, the fundamental frequency and the second and third harmonics, which are to be cancelled. The signal started at frequencies of 3 Hz, 6 Hz and 9 Hz, and changed to 4 Hz, 8 Hz and 12 Hz, then to 5 Hz, 10 Hz and 15 Hz over 120 seconds. Each transient period is 40 seconds, which is long enough to validate the response of the FXLMS controller with on-line secondary path identification. Similar to the multiple harmonics excitation, the overall peak input acceleration for each period is approximately 0.1 g. All the sub-controllers were switched on with zero initial gains and they were all fully adapted before the frequencies were changed.

Fig. 18 shows the comparison between the original vibration and the active cancellation result on the seat pan during the transient switching frequency period. It can be observed that the all the controllers are able to rapidly adapt the changing conditions and provide significant level of cancellation at the target frequencies. The initial adaption period is around 8 seconds, and after the controllers were fully adapted stable cancellation for each frequency is seen. Low level random noise which is introduced by the on-line FBLMS identification process is also shown in the cancellation spectrogram. However, this noise can be isolated passively by employing a seat cushion in practical application. Since this study's sole focus is the active cancellation system, passive cushion was not used in the experiments.

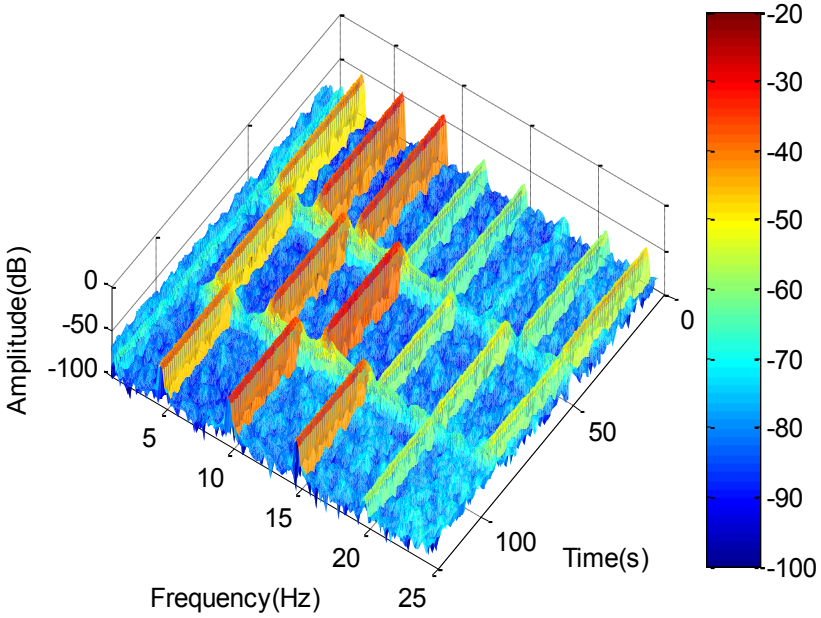

(a)

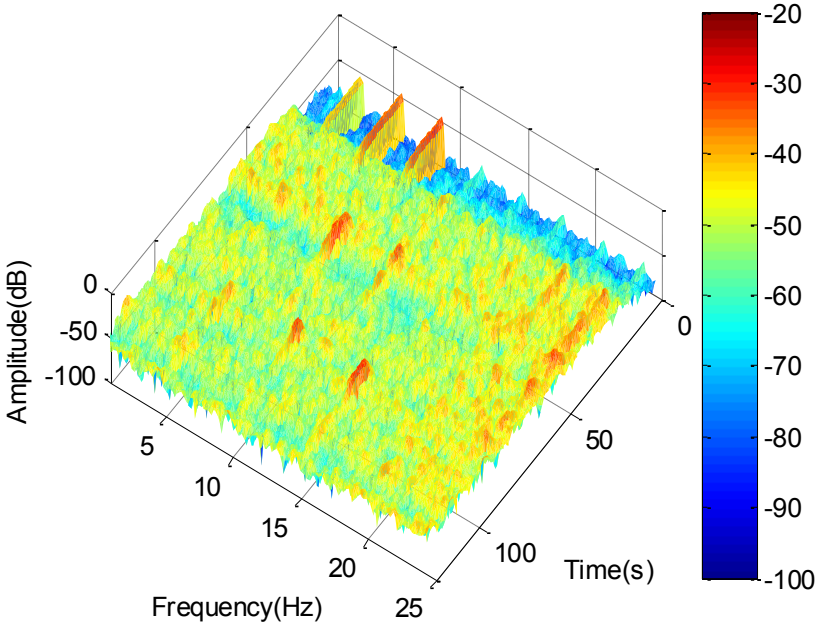

(b)

Fig. 18. Spectrograms of the original vibration and active cancellation result on the seat pan during the transient switching frequency period. (a) Original vibration; (b) after cancellation.

Fig. 19 and 20 show spectrograms of the original vibration and the cancellation results on the dummy pelvis and shoulder during the frequency switching period, respectively. As it can be seen, the vibration level on the dummy pelvis and shoulder is substantially reduced by the active control system at the target frequency. Also, a robust and rapid adaption during the frequency transient is confirmed.

As mentioned previously, in the above experimental tests the control algorithm only utilized the acceleration signal on the seat pan as the feedback error signal. This means the estimated secondary path only contains the dynamics of the active cancellation system, the dummy dynamics, therefore,

were not included. It can be expected that better cancellation performance can be achieved by taking the dummy dynamics into account.

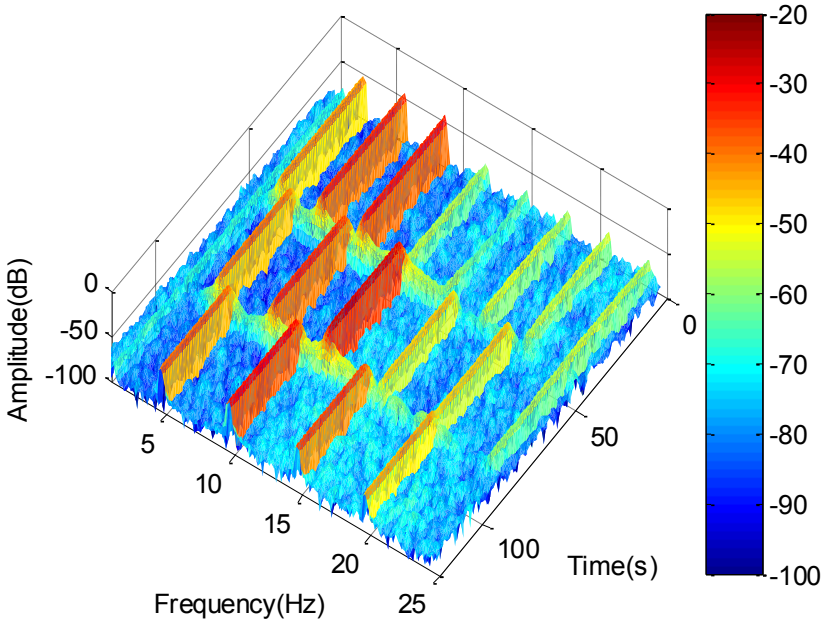

(a)

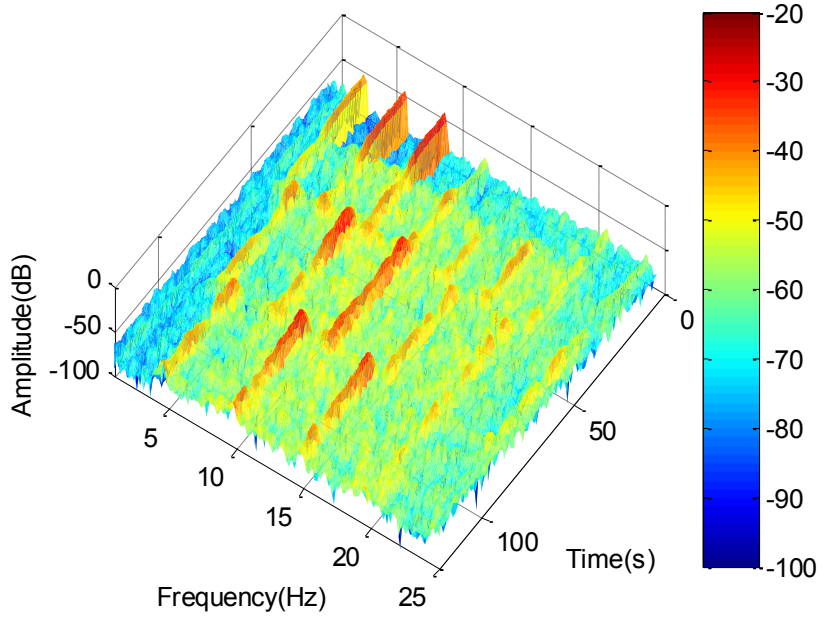

(b)

Fig. 19. Spectrograms of the original vibration and active cancellation result on the dummy pelvis during the transient switching frequency period. (a) Original vibration; (b) after cancellation.

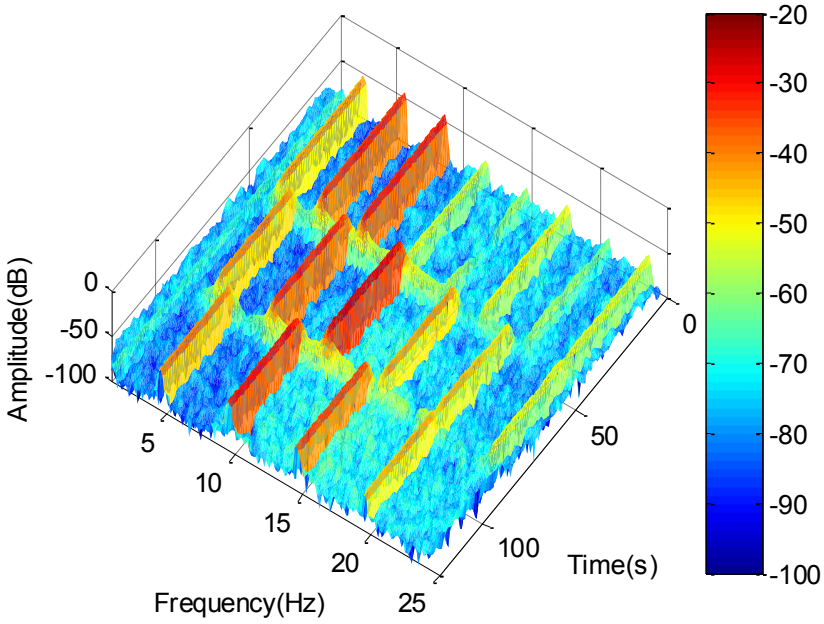

(a)

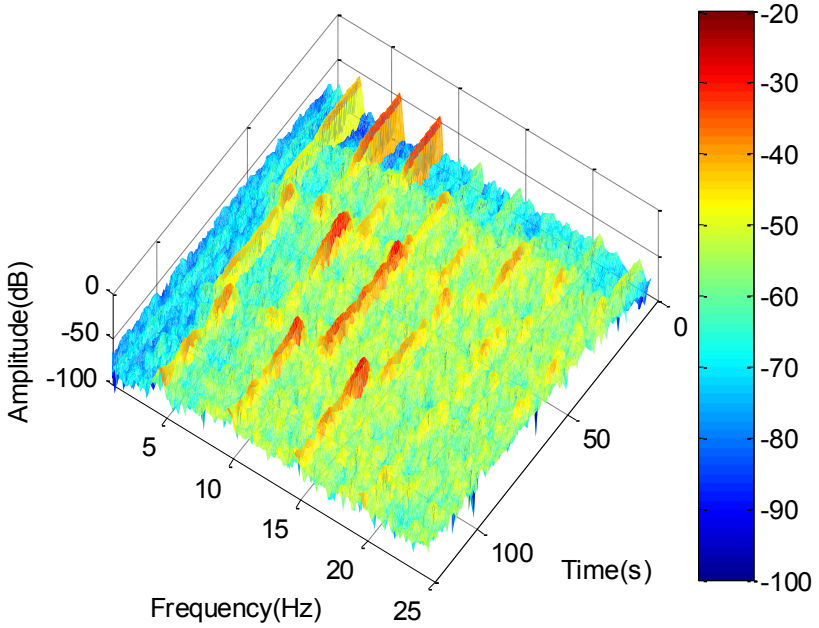

(b)

Fig. 20. Spectrograms of the original vibration and active cancellation result on the dummy shoulder during the transient switching frequency period. (a) Original vibration; (b) after cancellation.

6. Conclusions

A proof-of-concept active seat using electromagnetic linear actuators was proposed on the basis of the required high vibration isolation performance under low frequency periodic excitation. The detail of the mechanical structure was given and the active seat dynamics without external load were

characterized by vibration transmissibility and frequency responses under different excitation forces. Due to the fact that the active seat system is subject to non-linear and time-varying effects, the FXLMS adaptive control algorithm with on-line FBLMS identification process was employed to actively reduce the vibration transmitted from the floor to the seat pan and the occupants' body. An experimental test rig which can enable real-time implementation of the control algorithm was built in order to investigate the effectiveness of the active seat for vibration cancellation. The identification results revealed that an accurate estimation of the secondary path is achieved by using the on-line FBLMS technique. Effective performance was found for cancelling periodic vibration containing single and multiple frequencies. In addition, the robustness and stability of the control system were validated through transient switching frequency tests. To conclude, this study verified the effectiveness of the active seat and adaptive control approach to reduce occupants' vibration level under low frequency periodic excitation.

Acknowledgements

This work is supported by the University of Bath. Technical support from Alan Jefferis, Bernard Roe and Graham Rattley of the Centre for Power Transmission and Motion Control (CPTMC) is greatly appreciated.

References

[1] G.S. Paddan, M.J. Griffin, Evaluation of whole-body vibration in vehicle, *Journal of Sound and Vibration* 253 (1) (2002) 195–213.

[2] M.H. Pope, D.G. Wilder, M.L. Magnusson, A review of studies on seated whole body vibration and low back pain. *Proceedings of the Institution of Mechanical Engineers, Part H: Journal of Engineering in Medicine* (1999) 213-435.

[3] C. Hulshof, B. Veldhuijzen van Zanten, Whole-body vibration and low back pain - A review of epidemiologic studies. *International Archives of Occupational and Environmental Health* 59 （1987） 205-220.

[4] X. Wu, M.J. Griffin, A semi-active control policy to reduce the occurrence and severity of end-stop impacts in a suspension seat with an electrorheological fluid damper, *Journal of Sound and Vibration* 203 (1997) 781–793.

[5] S.B. Choi, M.H. Nam, B.K. Lee, Vibration control of a MR seat damper for commercial vehicles, *Journal of Intelligent Material Systems and Structures* 11 (2000) 936-944.

[6] S.J. McManus, K.A. St. Clair, P.E. Boileau, J. Boutin, Evaluation of vibration and shock attenuation performance of a suspension seat with a semi-active magnetorheological fluid damper, *Journal of Sound and Vibration* 253 (1) (2002) 313–327.

[7] G.J. Hiemenz, W. Hu, and N.M. Wereley, Semi-active magnetorheological helicopter crew seat suspension for vibration isolation, *Journal of Aircraft* 45 (2008) 945-953.

[8] M. Kawana and T. Shimogo, Active Suspension of Truck Seat, *Shock and Vibration* 5 (1) (1998) 35-41.

[9] G.J. Stein, A driver's seat with active suspension of electro-pneumatic type, *Journal of Vibration and Acoustics* 119(2) (1997) 230-235.

[10] I. Maciejewski, L. Meyer, T. Krzyzynski, The vibration damping effectiveness of an active seat suspension system and its robustness to varying mass loading, *Journal of Sound and Vibration* 329 (2010) 3898–3914.

[11] Y. Chen, V. Wickramasinghe and D.G. Zimcik, Development of adaptive helicopter seat for aircrew vibration reduction, *Journal of Intelligent Material Systems and Structures* (2011) 22-489.

[12] H. Li, H. Liu; H. Gao, P. Shi, Reliable fuzzy control for active suspension systems with actuator delay and fault, *IEEE Transactions on Fuzzy Systems* 20 (2) (2011) 342 – 357.

[13] A. Alleyne, J.K. Hedrick, Nonlinear adaptive control of active suspensions, *IEEE Transactions on Control Systems Technology* 3 (1) (2002) 94-101

[14] A.A. Aldair and W.J. Wang, A neurofuzzy controller for full vehicle active suspension systems, *Journal of Vibration and Control* 18 (2012) 1837-1854.

[15] J.D. Wu, R.J. Chen, Application of an active controller for reducing small-amplitude vertical vibration in a vehicle seat, *Journal of Sound and Vibration* 274 (2004) 939–951.

[16] I. Maciejewski, Control system design of active seat suspensions, *Journal of Sound and Vibration* 331 (2012) 1291–1309.

[17] I. Fialho and G. Balas, Road adaptive active suspension design using linear parameter-varying gain-scheduling*, IEEE Transactions on Control Systems Technology* 10 (1) (2002) 43–54.

[18] T.D. Le, K.K. Ahn, Active pneumatic vibration isolation system using negative stiffness structures for a vehicle seat, *Journal of Sound and Vibration* 333 (2014) 1245–1268.

[19] A.J. Hillis, A.J.L. Harrison, D.P. Stoten, A comparison of two adaptive algorithms for the control of active engine mounts, *Journal of Sound and Vibration* 286 (2005) 37–54.

[20] R. Guclu, Fuzzy logic control of seat vibrations of a non-Linear full vehicle model, *Nonlinear Dynamics* 40 (1) (2005) 21–34.

[21] P. Chen, A. Huang, Adaptive sliding control of non-autonomous active suspension systems with time-varying loadings, *Journal of Sound and Vibration* 282 (2005) 1119–1135.

[22] H. Gao, J. Lam, Ch. Wang, Multi-objective control of vehicle active suspension systems via load-dependent controllers, *Journal of Sound and Vibration* 290 (2006) 654–675.

[23] Y. Zhao, W. Sun, H. Gao, Robust control synthesis for seat suspension systems with actuator saturation and time-varying input delay, *Journal of Sound and Vibration* 329 (2009) 4335–4353.

[24] B. Widrow, M.E. Hoff, Adaptive switching circuits, *Proceedings of WESCON Convention Record* 4, Los Angeles, USA, 1960, pp. 96-140.

[25] S.M. Kuo, D.R. Morgan, *Active noise control systems: algorithms and DSP implementations*, John Wiley & Sons, New York, 1995.

[26] F.B. Behrouz, *Adaptive filters: theory and applications*, John Wiley & Sons, New York, 2013.